Path-Following Analysis of the Dynamical Response of a Piecewise-Linear Capsule System

Joseph Páez Chávez[c,d], Yang Liu[b,*], Ekaterina Pavlovskaia[a], Marian Wiercigroch[a]

[a] *Centre for Applied Dynamics Research, School of Engineering, University of Aberdeen, Aberdeen AB24 3UE, UK*
[b] *School of Engineering, Robert Gordon University, Aberdeen AB10 7GJ, UK*
[c] *Center for Dynamics, Department of Mathematics, TU Dresden, D-01062 Dresden, Germany*
[d] *Facultad de Ciencias Naturales y Matemáticas, Escuela Superior Politécnica del Litoral, Km. 30.5 Vía Perimetral, Guayaquil, Ecuador*

Abstract

The dynamical response of a piecewise-linear capsule system is studied by means of path-following techniques in this paper. As the capsule model belongs to the class of piecewise-smooth dynamical systems involving impact and friction, a special care is taken in order to divide the trajectory of the system into a smooth vector field in each disjoint subregion. Specifically we study a two-sided drifting system focusing on directional control and energy consumption. We aim to address two practical problems which are maximizing the rate of progression and directional control of the system by following a typical period-1 trajectory. The one-parameter analysis shows that two types of bifurcations, grazing bifurcation and boundary-intersection crossing bifurcation are found, and the maximal rate of progression is achieved when the capsule performs the oscillations without sticking phases. In our two-parameter study, the control parameters for which the rate of progression is maximal are identified using fixed value of power consumption, and the curves which divide the motion of the capsule between forward and backward progression are obtained.

Keywords: Capsule dynamics; Vibro-impact; Non-smooth dynamical system; Numerical continuation

1. Introduction

Rectilinear directional control of capsule robots [1–4] is a challenge task, particularly when dynamic environment is changing [5, 6]. In the application of capsule endoscopy [7, 8], extra legged mechanism is employed for the capsule in order to resist the natural peristalsis of gastrointestinal tract, e.g. [9, 10]. For the self-propulsion capsules, backward progression becomes a compulsory skill, and this could be achieved either through a careful design of the trajectory of the internal mass [1–3] or by suitably varying the oscillation parameters [4, 6, 11]. In the former case, the trajectory of the internal mass is limited by the size of the capsule, leading to complications in practical design. In the latter case, the internal mass is subject to a sinusoidal excitation and the motion can be controlled by varying the system parameters, such as the frequency and amplitude of harmonic excitation. However, determining the precise parameter values that allow changing the direction of the rectilinear motion is not straightforward, but can be done via dedicated studies of the dynamical response of capsule systems.

This paper presents a detailed analysis of the dynamical response of a vibro-impact capsule system, with special focus on its forward and backward progression. Such progression is sometimes referred to as a drift in the literature, which has received considerable attention in the past in the context of engineering applications, see e.g. [12–15]. In [12], the dynamics of a piecewise-linear drifting oscillator was studied and the analysis revealed that the largest drift was achieved when the system response switches from periodic

*Corresponding author. Tel. +44-1224-262420, e-mail: y.liu8@rgu.ac.uk.
Email addresses: jpaez@espol.edu.ec (Joseph Páez Chávez), e.pavlovskaia@abdn.ac.uk (Ekaterina Pavlovskaia), m.wiercigroch@abdn.ac.uk (Marian Wiercigroch)

to chaotic, originating from a cascade of period-doubling bifurcations. Luo and co-workers [13] considered a two-degrees-of-freedom plastic impact oscillator with a frictional slider, and the largest progression was found when the system operates under period-1, multi-impact motion. Ho et al. [14] studied the dynamic response of a electro-vibro-impact drifting system, and the highest progression rates and impact force of the system were achieved when periodic trajectories of the system occur. A novel drifting oscillator for analysis and prediction of percussive drilling was proposed by Depouhon et al. in [15]. In these previous investigations, only one-sided drift of the system has been considered. Therefore, the current paper aims at contributing to the study of two-sided drifting systems, with special emphasis on directional control and energy consumption.

The dynamical study of systems of the type considered here poses well-known challenges from a numerical point of view. These are mainly due to non-smooth nonlinearities, typical in systems involving impact and friction. In order to explore the behaviour of the capsule system, we will employ two different types of numerical approaches, namely, direct numerical integration and path-following techniques. As will be explained in detail later, the proposed capsule model belongs to the class of *piecewise-smooth dynamical systems* [16], which are characterized by periods of smooth evolution interrupted by instantaneous events. For this type of systems, the state space is usually divided into disjoint subregions, in such a way that the system dynamics in each region is described by a smooth vector field. Therefore, a special care must be taken in order to get reliable numerical approximations of the behaviour of such systems in an efficient way [17]. Path-following (continuation) methods are well-established techniques in applied mathematics [18] that enable a systematic study of a system response subject to parameter variations. For the case of piecewise-smooth systems, specialized continuation tools such as SlideCont [19], COCO [20] and TC-HAT [21] have been developed, and the latter will be employed in the current work for the numerical study of the capsule model.

The rest of the paper is organized as follows. In the next section, the physical model of the capsule system is explained and its equations of motion describing different modes of operation in a compact manner are presented. In Section 3, the mathematical formulation of the capsule model is studied in detail in order to carry out numerical analysis by means of TC-HAT. In particular, two solution measures are defined for monitoring the performance of the system. In Section 4, one-parameter analysis of the system under variation of excitation frequency is carried out by following a typical period-1 trajectory. Then two practical problems for which the rate of progression is maximised and directional control of the capsule system are tackled through two-parameter study. Finally, some concluding remarks are drawn in Section 5.

2. Physical Model and Equations of Motion

Consider a capsule system with two degrees of freedom as shown in Fig. 1. The system consists of a movable internal mass m_1 attached to an outer capsule of mass m_2 via a linear spring-damper pair k_1, c. The mass m_1 is subject to a harmonic excitation force with amplitude F_d and frequency Ω. The absolute displacements of the the internal mass and the capsule are given by the variables X_1 and X_2, respectively. If the relative displacement $X_1 - X_2$ exceeds a gap E, an intermittent contact between m_1 and a weightless plate attached to the capsule via a secondary spring k_2 takes place. When the resulting force acting on the capsule from the internal mass support and the secondary spring having stiffness k_2 is larger than the threshold of the Coulomb friction F_c between the capsule and its surrounding medium, a one-dimensional motion of the capsule occurs, whose direction depends on the direction of the resulting force within the capsule.

As will be explained in more detail in Section 3.1, the dynamics of the capsule system can be decomposed into various modes of operation, depending on whether the internal mass m_1 is in contact with the secondary k_2, direction of the capsule motion, etc. These operational modes can be mathematically

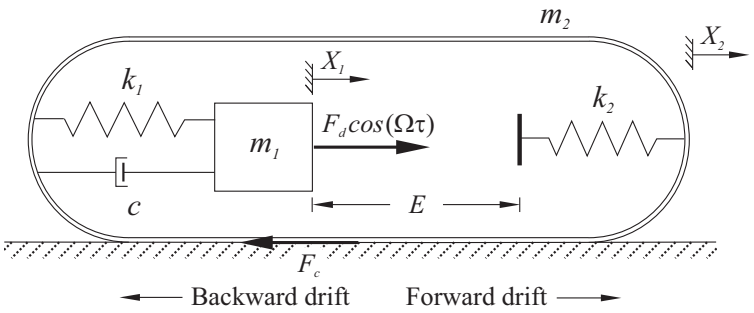

Figure 1: Physical model of the vibro-impact capsule system.

described in a compact form as follows (cf. [4, 6, 11]):

$$\begin{cases} x_1' = y_1, \\ y_1' = \alpha\cos(\omega t) + (x_2 - x_1) + 2\xi(y_2 - y_1) - P_3\beta(x_1 - x_2 - \delta), \\ x_2' = (P_1(1 - P_3) + P_2P_3)y_2, \\ y_2' = \dfrac{1}{\gamma}(P_1(1 - P_3) + P_2P_3)\left(P_3\beta(x_1 - x_2 - \delta) - (x_2 - x_1) - 2\xi(y_2 - y_1) - \mathrm{sign}(y_2)\right), \end{cases} \tag{1}$$

with $P_1 := H\left(\left|(x_2 - x_1) + 2\xi(y_2 - y_1)\right| - 1\right)$, $P_2 := H\left(\left|(x_2 - x_1) + 2\xi(y_2 - y_1) - \beta(x_1 - x_2 - \delta)\right| - 1\right)$ and $P_3 := H(x_1 - x_2 - \delta)$, where $H(\cdot)$ stands for the Heaviside step function. In the equations of motion (1), the following nondimensional variables and parameters have been introduced:

$$\begin{aligned} &\Omega_0 = \sqrt{\frac{k_1}{m_1}}, \quad && t = \Omega_0\tau, \quad && \omega = \frac{\Omega}{\Omega_0}, \quad && \xi = \frac{c}{2m_1\Omega_0}, \quad && \beta = \frac{k_2}{k_1}, \\ &\alpha = \frac{F_d}{F_c}, \quad && \delta = \frac{k_1}{F_c}E, \quad && \gamma = \frac{m_2}{m_1}, \quad && x_1 = \frac{k_1}{F_c}X_1, \quad && x_2 = \frac{k_1}{F_c}X_2. \end{aligned} \tag{2}$$

3. Capsule Model as a Piecewise-Smooth Dynamical System

As it is evident from the equations of motion (1), the capsule model belongs to the class of piecewise-smooth dynamical systems [16], which are characterized by periods of smooth evolution interrupted by instantaneous events. Typically, the trajectories of these systems are split into smooth segments consisting of the following components: a smooth vector field that governs the system behaviour during the segment and a smooth event function whose zeroes define the terminal point of the segment. Each segment is labeled with an index I_i, $i \in \mathbb{N}$, so that any solution of the piecewise-smooth dynamical system is fully characterized by its solution signature $\{I_i\}_{i=1}^{M}$, where $M \in \mathbb{N}$ defines the length of the signature. This mathematical formulation enables the application of path-following algorithms by means of the software package TC-HAT [21], a driver of AUTO 97 [22] for numerical continuation and bifurcation detection of periodic solutions of piecewise-smooth dynamical systems. Recent applications of TC-HAT can be found in [23–25], where the continuation package is employed to study the bifurcation scenario of particular engineering systems.

In order to write the periodically forced model as an autonomous system, the following standard nonlinear oscillator [18] will be appended to the equations of motion:

$$\begin{cases} r' = r + \omega s - r\left(r^2 + s^2\right), \\ s' = s - \omega r - s\left(r^2 + s^2\right), \end{cases} \tag{3}$$

which has the asymptotically stable solution, $r(t) = \sin(\omega t)$ and $s(t) = \cos(\omega t)$. This step is necessary

due to the AUTO 97-formulation which does not allow time-dependent forcing terms as that appearing in the capsule system (1). Furthermore, to decouple the periodic behaviour of the system from the (forward or backward) drift, we introduce the following linear transformation:

$$\begin{cases} w_1 = x_1, \\ w_2 = x_1 - x_2, \\ v_1 = y_1, \\ v_2 = y_1 - y_2. \end{cases} \tag{4}$$

Here, the new variables w_2 and v_2 give the position and velocity of the internal mass, respectively, relative to those of the capsule. In this way, the oscillatory motion of the system is fully described by the variables w_2, v_1 and v_2, as will be seen in the next section. This coordinate change is inspired by a previous work [26], in which the periodic and progressive motion of a drifting oscillator are detached so as to study the oscillatory modes separately.

3.1. Mathematical Formulation in TC-HAT

Denote by $\lambda := (\omega, \alpha, \xi, \delta, \beta, \gamma) \in \left(\mathbb{R}^+\right)^6$ and $u := (w_2, v_1, v_2, r, s)^T \in \mathbb{R}^5$ the parameters and the state variables of the system, respectively, with $\mathbb{R}^+$ being the set of positive numbers. Below we will introduce the segments I_{ij}, $i, j \in \mathbb{N}$, into which the trajectories of the piecewise-linear model (1) can be divided. Each segment will be associated with a smooth vector field and an event function, as explained at the beginning of Section 3.

No Contact - Stationary (NC-S), I_{11}, I_{12}, I_{13}. These segments occur when two conditions are met: the internal mass (m_1) and the secondary spring (k_2) are not in contact (see Fig. 1), and the force acting on the capsule from the internal mass support (k_1, c) is smaller than the threshold of the dry friction, that is

$$w_2 < \delta \quad \text{and} \quad |w_2 + 2\xi v_2| \leq 1.$$

The motion of the capsule during this regime is governed by the equation

$$u' = f_{\text{NC-S}}(u, \lambda) := \begin{pmatrix} v_1 \\ \alpha s - w_2 - 2\xi v_2 \\ \alpha s - w_2 - 2\xi v_2 \\ r + \omega s - r\left(r^2 + s^2\right) \\ s - \omega r - s\left(r^2 + s^2\right) \end{pmatrix}, \tag{5}$$

which is obtained after applying the coordinate transformation (4) to the equations of motion (1) and appending the nonlinear oscillator (3) to the resulting system. Note that in the original system (1) we have that $x_1' = y_1$ and $x_2' = 0$ (the capsule does not move). Combining this with the fact that $w_2' = x_1' - x_2'$ (see transformation (4)) gives $w_2' = v_1$, corresponding to the first component of (5). Moreover, this mode of operation terminates when one of the following events occur:

$$\begin{aligned} h_{11}(u, \lambda) &:= w_2 - \delta = 0 && \text{(Internal mass hits the secondary spring)}, \\ h_{12}(u, \lambda) &:= w_2 + 2\xi v_2 - 1 = 0 && \text{(Transition to forward drift)}, \\ h_{13}(u, \lambda) &:= w_2 + 2\xi v_2 + 1 = 0 && \text{(Transition to backward drift)}, \end{aligned}$$

where the subindex $1j$ refers to the segment labels I_{1j} introduced above, $j = 1, 2, 3$. In what follows, this notation will be used to associate the segment labels with the corresponding event functions.

No Contact - Forward Drift (NC-FD), I_{21}, I_{22}. These segments are characterized by the conditions:

$$w_2 < \delta \quad \text{and} \quad w_2 + 2\xi v_2 > 1,$$

i.e., the internal mass and the secondary spring are detached and the force acting on the capsule from the support of the internal mass exceeds the threshold of the dry friction in the forward direction. Hence, the capsule moves forward, and the dynamics of the system is described by

$$u' = f_{\text{NC-FD}}(u,\lambda) := \begin{pmatrix} v_2 \\ \alpha s - w_2 - 2\xi v_2 \\ \alpha s - (w_2 + 2\xi v_2)\left(1 + \frac{1}{\gamma}\right) + \frac{1}{\gamma} \\ r + \omega s - r\left(r^2 + s^2\right) \\ s - \omega r - s\left(r^2 + s^2\right) \end{pmatrix}. \tag{6}$$

This operation regime ends when one of the following events take place:

$$\begin{aligned} h_{21}(u,\lambda) &:= w_2 - \delta = 0 \quad \text{(Internal mass hits the secondary spring)}, \\ h_{22}(u,\lambda) &:= v_1 - v_2 = 0 \quad \text{(Capsule velocity becomes zero)}. \end{aligned}$$

No Contact - Backward Drift (NC-BD), I_{31}, I_{32}. This operation mode is analogous to the previous one, except that now the force acting on the capsule from the internal mass support exceeds the threshold of the dry friction in the backward direction. Thus, the conditions for this operation regime are

$$w_2 < \delta \quad \text{and} \quad w_2 + 2\xi v_2 < -1.$$

The motion of the capsule is described by the system of ODEs

$$u' = f_{\text{NC-BD}}(u,\lambda) := \begin{pmatrix} v_2 \\ \alpha s - w_2 - 2\xi v_2 \\ \alpha s - (w_2 + 2\xi v_2)\left(1 + \frac{1}{\gamma}\right) - \frac{1}{\gamma} \\ r + \omega s - r\left(r^2 + s^2\right) \\ s - \omega r - s\left(r^2 + s^2\right) \end{pmatrix}. \tag{7}$$

Similarly to the previous case, this mode of operation finishes when one of the events below occur:

$$\begin{aligned} h_{31}(u,\lambda) &:= w_2 - \delta = 0 \quad \text{(Internal mass hits the secondary spring)}, \\ h_{32}(u,\lambda) &:= v_1 - v_2 = 0 \quad \text{(Capsule velocity becomes zero)}. \end{aligned}$$

Contact - Stationary (C-S), I_{41}, I_{42}, I_{43}. These segments are analogous to those defined for the *No Contact - Stationary* mode. The difference is that now the internal mass is in contact with the secondary spring, hence an additional elastic force has to be considered in the conditions characterizing this operation regime:

$$w_2 \geq \delta \quad \text{and} \quad \left|w_2 + 2\xi v_2 + \beta(w_2 - \delta)\right| \leq 1.$$

The motion of the capsule is governed in this case by the system

$$u' = f_{\text{C-S}}(u,\lambda) := \begin{pmatrix} v_1 \\ \alpha s - w_2 - 2\xi v_2 - \beta(w_2 - \delta) \\ \alpha s - w_2 - 2\xi v_2 - \beta(w_2 - \delta) \\ r + \omega s - r\left(r^2 + s^2\right) \\ s - \omega r - s\left(r^2 + s^2\right) \end{pmatrix}. \tag{8}$$

This mode of operation terminates when one of the following events occur:

$$\begin{aligned} h_{41}(u,\lambda) &:= w_2 - \delta = 0 && \text{(Contact with the secondary spring is lost)}, \\ h_{42}(u,\lambda) &:= w_2 + 2\xi v_2 + \beta(w_2 - \delta) - 1 = 0 && \text{(Transition to forward drift)}, \\ h_{43}(u,\lambda) &:= w_2 + 2\xi v_2 + \beta(w_2 - \delta) + 1 = 0 && \text{(Transition to backward drift)}. \end{aligned}$$

Contact - Forward Drift (C-FD), I_{51}, I_{52}. This operation regime is characterized by the conditions:

$$w_2 \geq \delta \quad \text{and} \quad w_2 + 2\xi v_2 + \beta(w_2 - \delta) > 1,$$

analogously to the *No Contact - Forward Drift* mode. The capsule dynamics is described by the equation

$$u' = f_{\text{C-FD}}(u,\lambda) := \begin{pmatrix} v_2 \\ \alpha s - w_2 - 2\xi v_2 - \beta(w_2 - \delta) \\ \alpha s - \left(w_2(\beta+1) + 2\xi v_2\right)\left(1 + \frac{1}{\gamma}\right) + \frac{1}{\gamma}\left(\beta\delta(1+\gamma) + 1\right) \\ r + \omega s - r\left(r^2 + s^2\right) \\ s - \omega r - s\left(r^2 + s^2\right) \end{pmatrix}. \tag{9}$$

This operation regime ends when one of the events below take place:

$$\begin{aligned} h_{51}(u,\lambda) &:= w_2 - \delta = 0 \quad \text{(Contact with the secondary spring is lost)}, \\ h_{52}(u,\lambda) &:= v_1 - v_2 = 0 \quad \text{(Capsule velocity becomes zero)}. \end{aligned}$$

Contact - Backward Drift (C-BD), I_{61}, I_{62}. Similarly to the previous cases, this operation mode is analogous to its no-contact counterpart *(NC-BD)*. As before, the conditions characterizing this regime include the elastic force coming from the secondary spring

$$w_2 \geq \delta \quad \text{and} \quad w_2 + 2\xi v_2 + \beta(w_2 - \delta) < -1.$$

The motion of the capsule is described in this case by the system of ODEs

$$u' = f_{\text{C-BD}}(u,\lambda) := \begin{pmatrix} v_2 \\ \alpha s - w_2 - 2\xi v_2 - \beta(w_2 - \delta) \\ \alpha s - \left(w_2(\beta+1) + 2\xi v_2\right)\left(1 + \frac{1}{\gamma}\right) + \frac{1}{\gamma}\left(\beta\delta(1+\gamma) - 1\right) \\ r + \omega s - r\left(r^2 + s^2\right) \\ s - \omega r - s\left(r^2 + s^2\right) \end{pmatrix}. \tag{10}$$

This mode of operation finishes when one of the following events occur:

$$\begin{aligned} h_{61}(u,\lambda) &:= w_2 - \delta = 0 \quad \text{(Contact with the secondary spring is lost)}, \\ h_{62}(u,\lambda) &:= v_1 - v_2 = 0 \quad \text{(Capsule velocity becomes zero)}. \end{aligned}$$

In Table 1 we summarize the operation modes and segments defined above. An illustration of this orbit segmentation is presented in Fig. 2. Finally, the capsule model can be expressed in terms of the vector fields introduced before as follows:

No contact ($w_2 < \delta$):

$$u' = \begin{cases} f_{\text{NC-S}}(u,\lambda), & v_1 - v_2 = 0 \ \text{ and } \ |w_2 + 2\xi v_2| \leq 1, \\ f_{\text{NC-FD}}(u,\lambda), & v_1 - v_2 > 0 \ \text{ or } \ (v_1 - v_2 = 0 \ \text{ and } \ w_2 + 2\xi v_2 > 1), \\ f_{\text{NC-BD}}(u,\lambda), & v_1 - v_2 < 0 \ \text{ or } \ (v_1 - v_2 = 0 \ \text{ and } \ w_2 + 2\xi v_2 < -1). \end{cases} \tag{11}$$

Contact ($w_2 \geq \delta$):

$$u' = \begin{cases} f_{\text{C-S}}(u,\lambda), & v_1 - v_2 = 0 \ \text{ and } \ \left|w_2 + 2\xi v_2 + \beta(w_2 - \delta)\right| \leq 1, \\ f_{\text{C-FD}}(u,\lambda), & v_1 - v_2 > 0 \ \text{ or } \ \left(v_1 - v_2 = 0 \ \text{ and } \ w_2 + 2\xi v_2 + \beta(w_2 - \delta) > 1\right), \\ f_{\text{C-BD}}(u,\lambda), & v_1 - v_2 < 0 \ \text{ or } \ \left(v_1 - v_2 = 0 \ \text{ and } \ w_2 + 2\xi v_2 + \beta(w_2 - \delta) < -1\right). \end{cases} \tag{12}$$

Operation mode	Segment	Vector field	Event function
No Contact - Stationary (NC-S)	I_{11}	$f_{\text{NC-S}}$	h_{11}
	I_{12}	$f_{\text{NC-S}}$	h_{12}
	I_{13}	$f_{\text{NC-S}}$	h_{13}
No Contact - Forward Drift (NC-FD)	I_{21}	$f_{\text{NC-FD}}$	h_{21}
	I_{22}	$f_{\text{NC-FD}}$	h_{22}
No Contact - Backward Drift (NC-BD)	I_{31}	$f_{\text{NC-BD}}$	h_{31}
	I_{32}	$f_{\text{NC-BD}}$	h_{32}
Contact - Stationary (C-S)	I_{41}	$f_{\text{C-S}}$	h_{41}
	I_{42}	$f_{\text{C-S}}$	h_{42}
	I_{43}	$f_{\text{C-S}}$	h_{43}
Contact - Forward Drift (C-FD)	I_{51}	$f_{\text{C-FD}}$	h_{51}
	I_{52}	$f_{\text{C-FD}}$	h_{52}
Contact - Backward Drift (C-BD)	I_{61}	$f_{\text{C-BD}}$	h_{61}
	I_{62}	$f_{\text{C-BD}}$	h_{62}

Table 1: Segments defined for the numerical study of the capsule model in TC-HAT.

3.2. Solution Measures

In this section we will introduce two solution measures that will be used to monitor the changes in the periodic response of the capsule system when a control parameter is varied. In most of the path-following packages (e.g. AUTO 97 [22]), the L_2-norm is set by default as the principal solution measure to construct bifurcation diagrams. Nevertheless, in our study we will use solution measures that allow us to gain more insight into the physical phenomena occurring in the capsule system.

From a practical point of view, one of the main concerns in capsule applications is to investigate the influence of the control parameters on the average rate of progression (drift) per period of the capsule, which can be computed as follows. Consider a periodic solution $u(t) = (w_2(t), v_1(t), v_2(t), r(t), s(t))$ of (11)–(12) with period $T > 0$. We thus define the rate of progression as (see (1) and (4))

$$\text{ROP} := \frac{1}{T}\int_0^T (v_1(t) - v_2(t))\, dt, \tag{13}$$

whose sign indicates whether the capsule moves forward (positive ROP) or backward (negative ROP).

The second solution measure that will be used in our study is related to the average power dissipated by the capsule system per period, defined as

$$P_{\text{AVG}} := \frac{1}{T}\int_0^T \alpha\cos(\omega t)v_1(t)\, dt = \frac{1}{T}\int_0^T \alpha s(t)v_1(t)\, dt. \tag{14}$$

The quantities (13) and (14) defined above will allow us to tackle practical questions, such as finding the parameter values yielding the highest progression rates, optimal operation conditions in terms of energy consumption, parametric boundaries between forward and backward drift, etc.

4. Numerical Investigation of the Capsule Dynamics

As mentioned earlier, one of our main concerns is to investigate the drift of the capsule and its energy consumption, for which reason the solution measures ROP and P_{AVG} defined before will be monitored in the following bifurcation study. For this purpose path-following methods will be applied, using the period-1 trajectory shown in Fig. 2 as starting solution, for which the capsule presents forward drift with stick and slip phases with short periods of backward motion. In Section 4.1, we will begin our

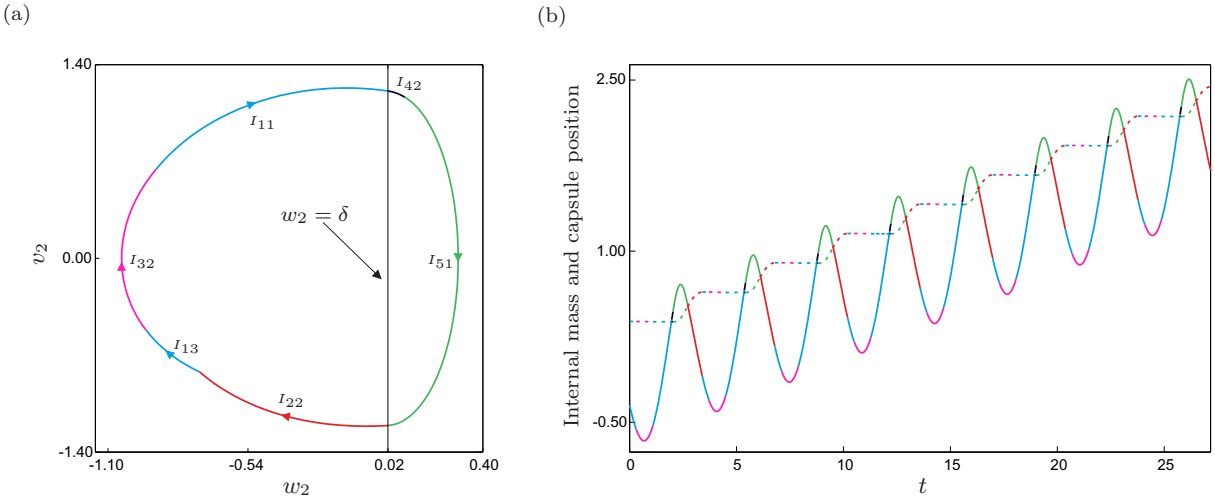

Figure 2: Period-1 solution of the capsule system (11)–(12) computed for the parameter values $\omega = 1.85$, $\alpha = 0.6$, $\xi = 0.05$, $\delta = 0.02$, $\beta = 12$ and $\gamma = 3$. Panel (a) shows the segments I_{22} (*No Contact - Forward Drift*), I_{13} (*No Contact - Stationary*), I_{32} (*No Contact - Backward Drift*), I_{11} (*No Contact - Stationary*), I_{42} (*Contact - Stationary*) and I_{51} (*Contact - Forward Drift*), listed in Table 1. Hence, the displayed trajectory has a cyclic solution signature $\{I_{22}, I_{13}, I_{32}, I_{11}, I_{42}, I_{51}\}$. Panel (b) depicts the corresponding time history showing the internal mass (solid line) and capsule (dashed line) motion. The colors denote the orbit segments as displayed in panel (a).

analysis with a detailed one-parameter study with respect to the excitation frequency ω, and identify the maximum average power dissipated by the system and the maximum rate of progression. In Section 4.2, the two-parameter continuation with respect to the excitation frequency ω and the mass ratio γ will be carried out by keeping the average power consumption P_{AVG} as a constant. In this way, we will try to identify the parameter scenarios for which the capsule system is operating in the energy-efficient manner.

4.1. One-parameter analysis

From a practical point of view, one of the main concerns is to maximize the rate of progression of the capsule system while minimising consumption of energy. Therefore, we will first perform the numerical continuation of the periodic orbit shown in Fig. 2 with respect to the frequency of excitation ω by using ROP and P_{AVG} as solution measures. The result of the continuation is depicted in Fig. 3 where two types of bifurcations, grazing (labeled GRi) and boundary-intersection crossing (labeled BCi), have been found. The latter type usually takes place when two discontinuity boundaries, say H_1 and H_2, intersect each other transversely in the state space. If a periodic solution passes through a point in the intersection $H_1 \cap H_2$ upon variation of a single parameter, then this event is called a boundary-intersection crossing bifurcation. A more detailed discussion about this phenomenon and its dynamical implications can be found in [27, Section 2.3] and [16, Section 7.3].

The sequence of bifurcations shown in Fig. 3(a) is as follows. First, at $\omega \approx 1.4526$ we found the grazing bifurcation GR1, for which a period-1 solution of the capsule system makes grazing contact with the discontinuity boundary $w_2 + 2\xi v_2 = -1$, as will be explained in more detail later. The first boundary-intersection crossing bifurcation is found at $\omega \approx 1.5068$, which is produced by a solution trajectory passing through a point in the intersection of the discontinuity boundaries $v_1 - v_2 = 0$ and $w_2 + 2\xi v_2 = -1$. Another boundary-intersection crossing bifurcation is encountered for $\omega \approx 1.6648$ (BC2), whose detailed description will be given later. The transversal intersection of the discontinuity boundaries $v_1 - v_2 = 0$ and $w_2 + 2\xi v_2 + \beta(w_2 - \delta) = 1$ gives rise to the bifurcation BC3 ($\omega \approx 1.6955$), after which the stick-slip motion of the capsule system disappears. As the excitation frequency is further increased, additional bifurcation points BC4, BC5, and BC6 are detected at $\omega \approx 1.7599$, 1.7771, and 1.8294, respectively. After BC4 the motion of capsule presents again stick and slip phases with small intervals of backward drift. This backward motion, however, disappears at $\omega \approx 1.8594$ via the grazing bifurcation GR2. After this point, the last boundary-intersection crossing bifurcation BC7 is found at $\omega \approx 2.0911$. If the excitation frequency

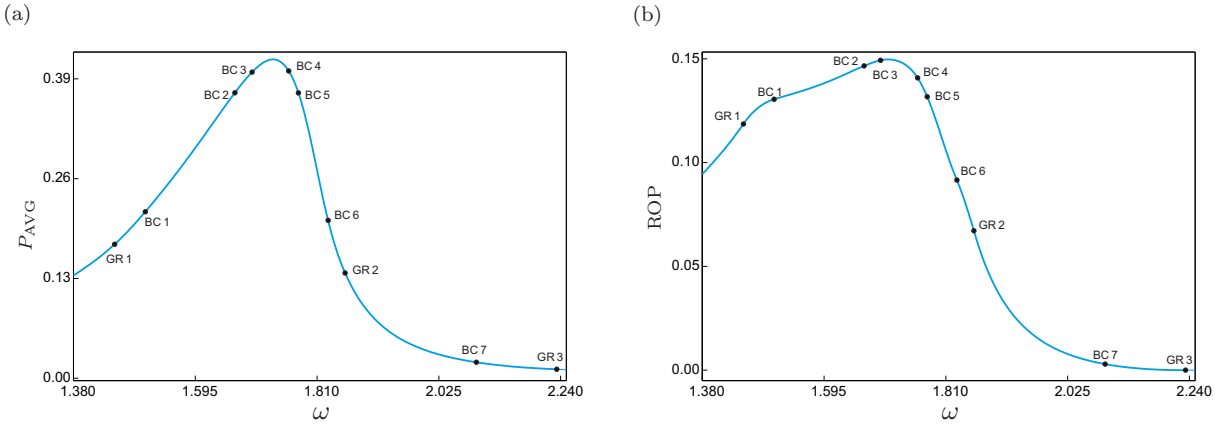

Figure 3: One-parameter continuation of the period-1 response of the capsule system (11)–(12) with respect to the excitation frequency ω, computed for the parameter values $\alpha = 0.6$, $\xi = 0.05$, $\delta = 0.02$, $\beta = 12$ and $\gamma = 3$. Panels (a) and (b) show the behaviour of the average power consumption P_{AVG} and the rate of progression ROP, respectively, as the frequency varies. The points labeled GRi denote grazing bifurcations, while BCi represent boundary-intersection crossing bifurcations detected during the continuation process.

is further increased, the ROP becomes smaller and smaller until it reaches zero at the bifurcation point GR3 ($\omega \approx 2.2331$), for which a period-1 orbit makes grazing contact with the discontinuity boundary $w_2 + 2\xi v_2 + \beta(w_2 - \delta) = 1$, which defines the transition to forward drift during the contact mode. It should be noted that the capsule system has the oscillations without sticking phases for $\omega \in (1.696, 1.76)$, i.e. between BC3 and BC4 as shown in panel (b), and the maximum ROP and P_{AVG} are both achieved at $\omega \approx 1.714$ and 1.732, respectively.

In Fig. 4 we show in more detail the dynamics of the capsule around the bifurcation point GR1, detected at $\omega \approx 1.4526$. In panel (a) we can observe the solution trajectory making grazing contact with the discontinuity boundary $w_2 + 2\xi v_2 = -1$, which defines the transition to backward motion during the no contact mode. For frequency values before GR1 (see panel (b)), the capsule motion is characterized by a classical stick-slip response, as can be verified by observing the time history of the capsule velocity, which is always ≥ 0. This behaviour persists up to the bifurcation point GR1, after which the solution crosses the discontinuity boundary $w_2 + 2\xi v_2 = -1$, hence giving rise to small intervals of backward motion. This effect can be clearly observed in panel (c), which shows the system response for $\omega = 1.49$ (after GR1). From a practical point of view, such bifurcations can be extremely dangerous, for instance in medical applications where capsule robots are used to explore veins and arteries, in which case backward motions of the capsule must be avoided to prevent damage of the tissue. Furthermore, such small backward drifts may also affect the efficiency of the system due to energy dissipated through friction.

Fig. 5 shows the behaviour of the capsule system near the boundary-intersection crossing bifurcation BC2, found at $\omega = \omega_{\mathrm{BC}} \approx 1.6648$. As explained before, such bifurcations take place when two discontinuity boundaries intersect each other transversely in the state space. In our particular case, these boundaries are $v_1 - v_2 = 0$ and $w_2 = \delta$, which, for the sake of clarity, will be referred to as H_1 and H_2, respectively. Panel (c) presents a small portion of the state space around the intersection $H_1 \cap H_2$, for $\omega < \omega_{\mathrm{BC}}$, showing the segment sequence $\{I_{32}, I_{11}, I_{42}, I_{51}\}$ (see Table 1). If the frequency slightly increases, the length of the segment I_{11} gradually decreases and then disappears at $\omega = \omega_{\mathrm{BC}}$. At this point, the terminal point of the segment I_{31} shown in panel (b) belongs to the intersection $H_1 \cap H_2$, which precisely characterizes the boundary-intersection crossing bifurcation. After $\omega = \omega_{\mathrm{BC}}$, a new segment I_{62} is created, whose length locally grows as the frequency increases, and the solution presents the segment sequence $\{I_{31}, I_{62}, I_{42}, I_{51}\}$ around $H_1 \cap H_2$. This is a typical scenario for a boundary-intersection crossing bifurcation, around which the solution segmentation experiences dramatic changes upon small variations of a parameter [16, 27].

4.2. Two-parameter analysis

In this section we will make use of the TC-HAT capability for two-parameter continuation of periodic solutions with an additional boundary condition. In our study, this additional condition will be given

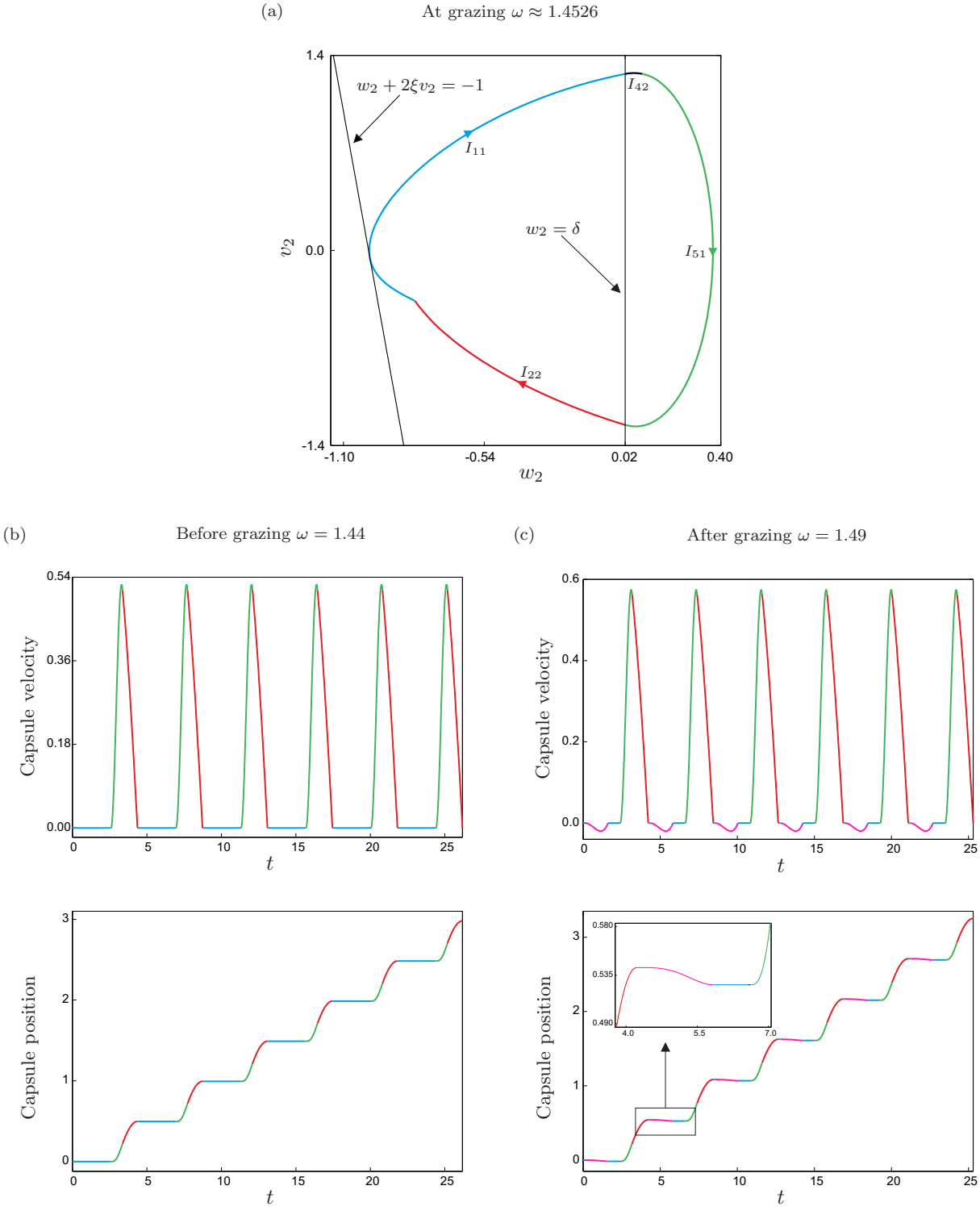

Figure 4: (a) Grazing orbit of system (11)–(12) corresponding to the bifurcation point GR1 shown in Fig. 3. (b) Time histories of the capsule velocity and position for $\omega = 1.44$, before grazing occurs. (c) Time histories of the capsule velocity and position for $\omega = 1.49$, after grazing. The boxed region shows that in this operation mode there is a time window for which the capsule moves backward, corresponding to the interval in which the capsule velocity is negative.

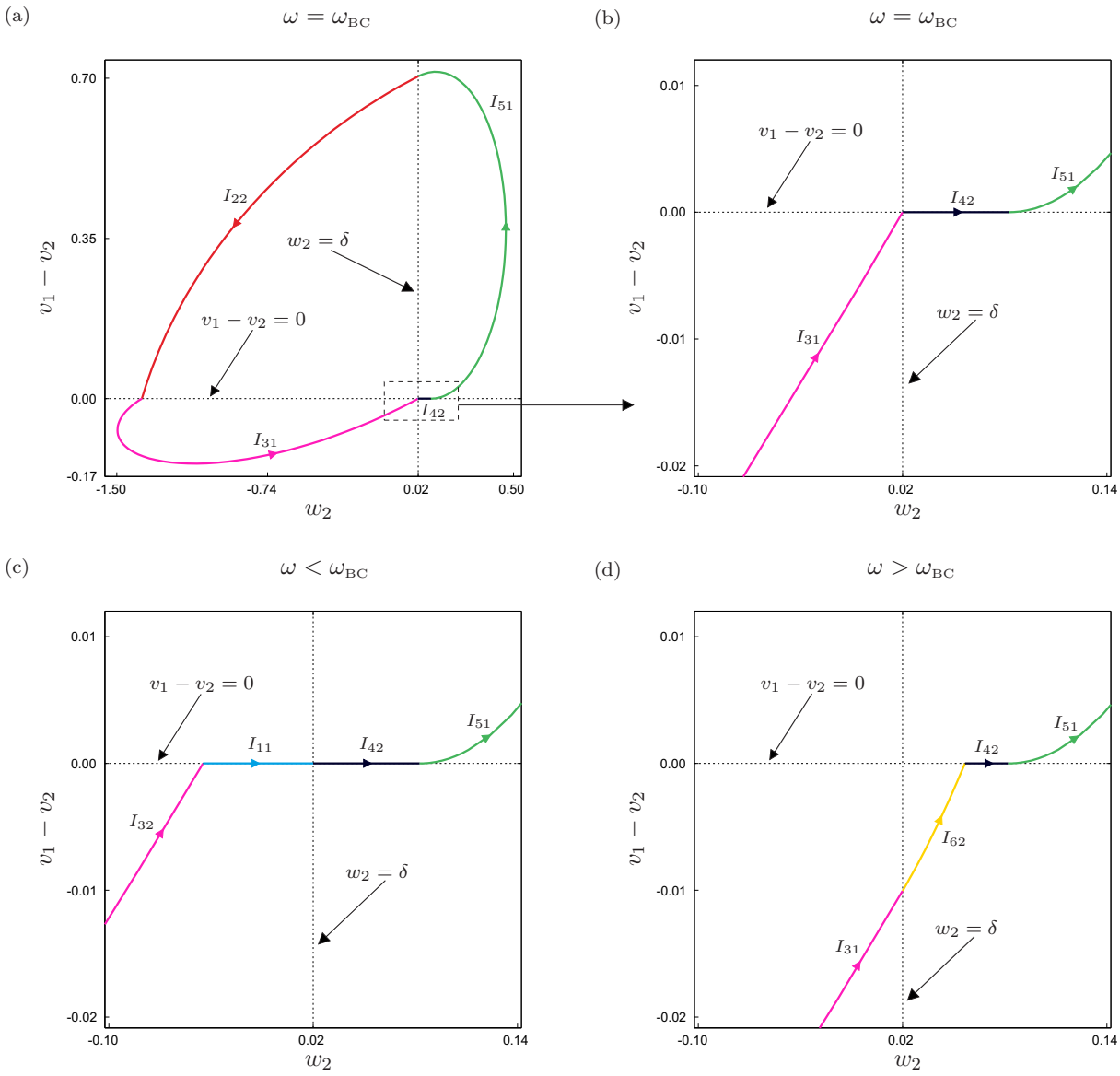

Figure 5: Behaviour of the periodic response of the system (11)–(12) around the boundary-intersection crossing bifurcation BC2 ($\omega = \omega_{\rm BC} \approx 1.6648$) shown in Fig. 3. (a) Orbit computed for $\omega = \omega_{\rm BC}$. (b) Enlargement of the boxed region depicted in panel (a). Panels (c) and (d) show the orbit segmentation within the boxed region before ($\omega = 1.645$) and after ($\omega = 1.680$) the boundary-intersection crossing bifurcation, respectively.

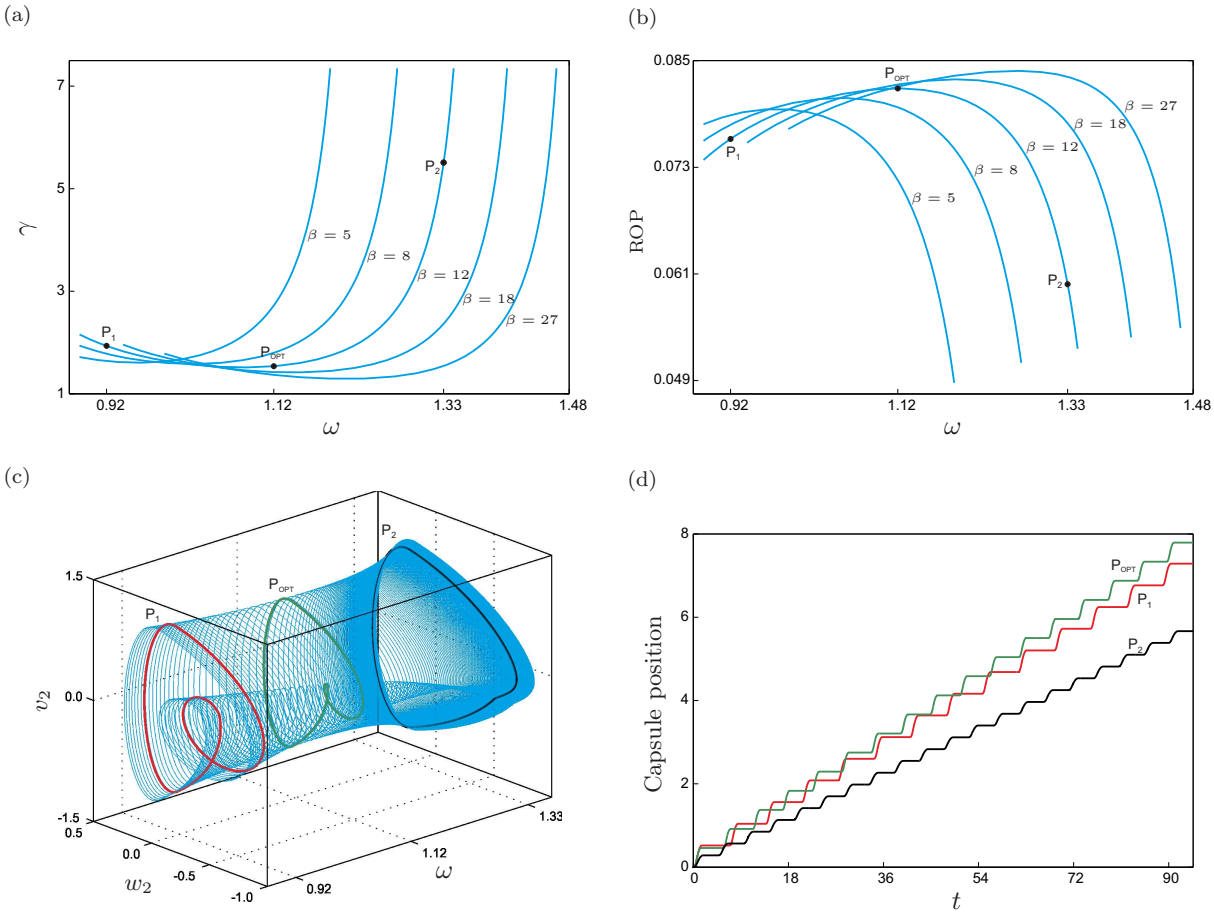

Figure 6: Two-parameter continuation of the periodic orbits for the system (11)–(12) with respect to the excitation frequency ω and the mass ratio γ, computed for the parameter values $\alpha = 0.6$, $\xi = 0.05$, $\delta = 0.02$, and $\beta = 5, 8, 12, 18, 27$. (a) Resulting curves in the ω-γ plane for which the average power consumption $P_{\text{AVG}} = 0.1$ is kept constant. (b) Behaviour of the ROP along the constant-power curves shown in panel (a). The label P_{OPT} marks the point of highest ROP for the case $\beta = 12$. (c) Solution family computed along the constant-power curve when $\beta = 12$. (d) Capsule motion computed at the points P_1 ($\omega = 0.92$, $\gamma = 1.9330$), P_{OPT} ($\omega \approx 1.1225$, $\gamma \approx 1.5376$) and P_2 ($\omega = 1.3280$, $\gamma = 5.5019$) shown in panels (a), (b) and (c), corresponding to the case $\beta = 12$.

in terms of the solutions measures (13) and (14), which are related to the rate of progression (ROP) and average power dissipated by the capsule (P_{AVG}), respectively. The first question we are going to tackle with this approach concerns the maximization of the ROP with a prescribed power consumption. Specifically, we will perform the numerical continuation of a periodic orbit of the capsule system with respect to the frequency of excitation ω and the mass ratio γ, with the condition $P_{\text{AVG}} = 0.1$. As we do so, we will monitor the behaviour of the ROP and determine the parameter values for which a maximum has been achieved. The result of this numerical procedure can be seen in Fig. 6(a), showing a family of curves with different stiffness ratios in the ω-γ plane for which the power consumption of the capsule is exactly $P_{\text{AVG}} = 0.1$. Panel (b) presents the values of ROP along the power curves described before. Here, for $\beta = 12$, we determined that the ROP achieves a maximum value ≈ 0.0819 at $(\omega, \gamma) \approx (1.1225, 1.5376)$. In panel (c), we depict the family of periodic solutions projected onto the w_2-v_2, computed along the power curve. In addition, we computed the capsule motion for three points: P_1 ($\omega = 0.92$, $\gamma = 1.9330$), P_{OPT} ($\omega \approx 1.1225$, $\gamma \approx 1.5376$, giving the maximum ROP) and P_2 ($\omega = 1.3280$, $\gamma = 5.5019$). The result is shown in panel (d), in which it can be verified that at P_{OPT} the capsule moves indeed faster than for the other parameter combinations at P_1 and P_2. Another observation from panel (b) is that, as the stiffness ratio β increases, the value of ROP at P_{OPT} is getting larger so that the capsule becomes more efficient.

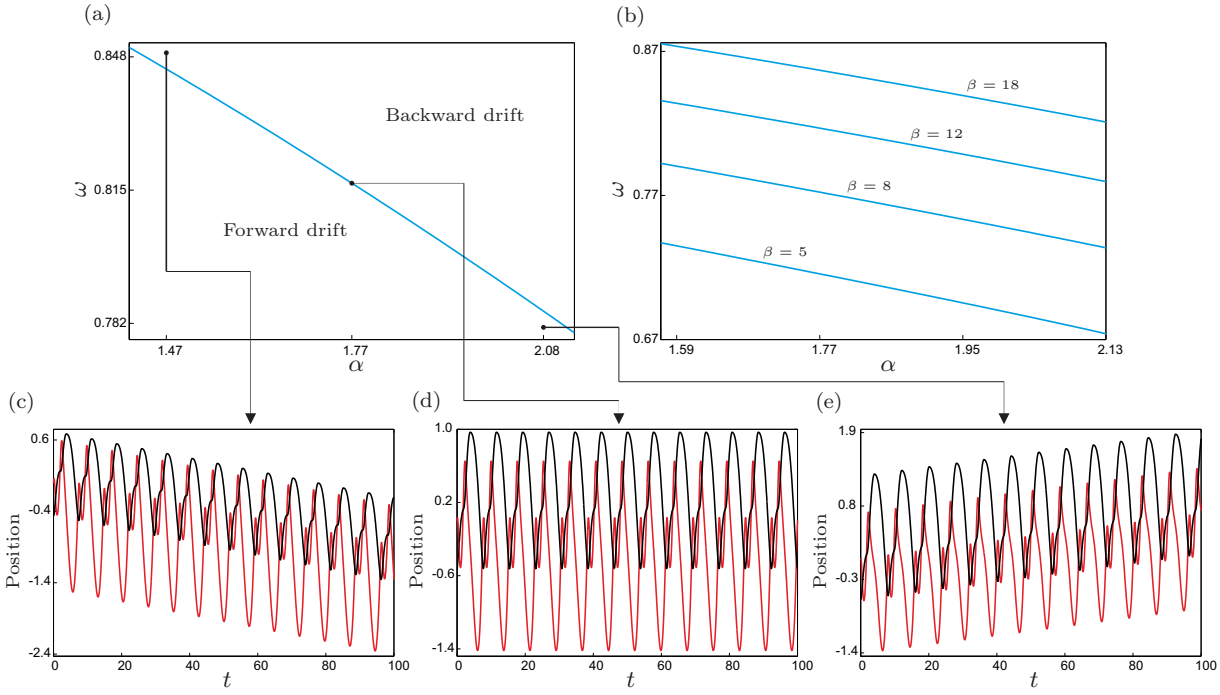

Figure 7: Two-parameter continuation of the periodic orbits for the system (11)–(12) with respect to the amplitude α and frequency ω of excitation, computed for the parameter values $\xi = 0.05$, $\delta = 0.02$, $\gamma = 3$ and $\beta = 5, 8, 12, 18$. (a) Resulting curve in the α-ω plane along which the ROP is zero, for $\beta = 12$. (b) Family of zero-ROP curves for the stiffness ratios indicated in the picture. (c) Backward drift of the capsule system for $\alpha = 1.47$, $\omega = 0.849$, $\beta = 12$. (d) Zero-drift of the capsule system for $\alpha = 1.77$, $\omega \approx 0.8167$, $\beta = 12$. (e) Forward drift of the capsule system for $\alpha = 2.08$, $\omega = 0.781$, $\beta = 12$. In panels (c), (d) and (e), the red and black lines represent the motion of the internal mass and the capsule, respectively.

Another practical issue that can be addressed in the framework of two-parameter continuation is that of directional control. Preliminary studies on this topic has been carried out by the authors in the past (Liu et al. [6] and [4]), where the directional control was achieved by judiciously varying the mass ratio γ or by switching between coexisting attractors. In the present work, we will employ a different approach based on path-following techniques. As mentioned earlier, the ROP, as defined in (13), can take negative, zero and positive values, which in turn indicate the direction of capsule drift (or no drift). Therefore, a continuous control of the drift direction can be implemented when the operating point of the capsule is set around ROP = 0. Similarly as before, this can be determined by performing the two-parameter continuation of a periodic solution with the additional condition ROP = 0. The result of this process is presented in Fig. 7(a), showing a curve in the α-ω plane for which the ROP is exactly zero. This curve divides locally the two-parameter space into three regions: forward drift (ROP > 0, below the curve), zero drift (ROP = 0, on the curve), and backward drift (ROP < 0, above the curve). This can be verified in panels (c), (d) and (e), which depicts the capsule motion for backward, zero and forward drift, respectively. A family of these curves for various stiffness ratio β are presented in panel (b), and the results show that, as the stiffness ratio increases, the frequency and the amplitude of excitation need to be larger in order to control the direction of capsule drift.

5. Conclusions and Future Work

The dynamical response of a piecewise-linear capsule system was studied by means of path-following techniques in this paper. As the capsule model belongs to the class of piecewise-smooth dynamical systems involving impact and friction, the trajectory of the system was split into smooth segments consisting a smooth vector field that governed the system behaviour during the segment and a smooth event function whose zeroes defined the terminal point of the segment. Therefore, a special care was taken in order to

get reliable numerical approximations of the behaviour of such system in an efficient way. The novelty of our contribution comes from the fact that this is the first study of a two-sided capsule drifting system, where we paid a special attention on directional control and energy consumption. Two practical issues of maximizing the rate of progression and directional control were tackled by using the continuation tool TC-HAT to follow a typical period-1 trajectory of the capsule system. Two solution measures, the rate of progression ROP and the average power dissipated by the capsule system P_{AVG} were defined for monitoring the performance of the system.

Our one-parameter study was undertaken by performing the numerical continuation of the period-1 orbit with respect to the frequency of excitation ω. The result of the continuation shows two types of bifurcations, i.e. grazing bifurcation and boundary-intersection crossing bifurcation. The grazing bifurcations were produced via a tangential contact with the discontinuity boundaries $w_2+2\xi v_2+\beta(w_2-\delta)=1$ and $w_2+2\xi v_2=-1$, which define the transition to forward (in the contact case) and backward (no contact), respectively. The transversal intersection between the boundaries $v_1-v_2=0$ and $w_2=\delta$ gave rise to a boundary-intersection crossing bifurcation that was studied in detail. The numerical continuation indicates that the capsule system has small periods of negative capsule velocity in which case the capsule moves a little bit backward when the first grazing bifurcation GR1 is encountered. As the frequency of excitation increases, the backward drift of the capsule disappears entirely after the second grazing bifurcation GR2, and when the third one GR3 is encountered, the capsule has no progression thereafter. Our findings show that the capsule system performs the oscillations without sticking phases for $\omega \in (1.696, 1.76)$ which is between the third BC3 and the fourth boundary-intersection crossing bifurcation BC4, and the maximum ROP and P_{AVG} could both be achieved at $\omega \approx 1.714$ and 1.732, respectively.

In our two-parameter study, in order to find the maximum ROP using limited power, we fixed a value of power consumption $P_{\text{AVG}}=0.1$ and found the curves for different stiffness ratios in ω-γ plane producing exactly the same power consumption via continuation. Then we computed the ROP along each curve and obtained the maximal ROP. For $\beta=12$, we have identified the maximal ROP at $\omega\approx 1.1225$, $\gamma\approx 1.5376$. As the stiffness ratio β increases, the maximal ROP along each curve is getting larger so that the capsule system becomes more efficient. For the directional control of the capsule system, we carried out first the numerical continuation of a periodic solution with respect to the amplitude of excitation α, and found a point for which the ROP changed sign. Then by including the additional condition ROP$=0$ in the continuation routine, the continuation was carried out in the α-ω plane and the curve was obtained. This curve divides the α-ω plane into three modes of operation, i.e. forward drift, zero drift, and backward drift. Therefore, the capsule system can be driven along a desired direction by a proper selection of the control parameters, α and ω. We also calculated a series of these curves for various stiffness ratios, and our findings show that, as the stiffness ratio β increases, the frequency and the amplitude of excitation need to be larger in order to control the direction of capsule progression.

Acknowledgements

The first author has been supported by a Georg Forster Research Fellowship granted by the Alexander von Humboldt Foundation, Germany.

References

[1] Y. Liu, H. Yu, and T. C. Yang, "Analysis and control of a Capsubot," in *Proceedings of IFAC World Congress*, (Seoul, Korea), pp. 756–761, 2008.

[2] F. L. Chernousko, "The optimal periodic motions of a two-mass system in a resistant medium," *J. Appl. Math. Mech.*, vol. 72, pp. 116–125, 2008.

[3] H. B. Fang and J. Xu, "Dynamics of a mobile system with an internal acceleration-controlled mass in a resistive medium," *Journal of Sound and Vibration*, vol. 330, pp. 4002–4018, 2011.

[4] Y. Liu, E. E. Pavlovskaia, M. Wiercigroch, and Z. K. Peng, "Forward and backward motion control of a vibro-impact capsule system," *Int. J. Non-Linear Mech.*, vol. 70, pp. 30–46, 2015.

[5] C. Zhang, H. Liu, R. Tan, and H. Li, "Modeling of velocity-dependent frictional resistance of a capsule robot inside an intestine," *Tribol Lett*, vol. 47, pp. 295–301, 2012.

[6] Y. Liu, E. E. Pavlovskaia, D. Hendry, and M. Wiercigroch, "Vibro-impact responses of capsule system with various friction models," *Internat. J. of Mech. Sci.*, vol. 72, pp. 39–54, 2013.

[7] T. Nakamura and A. Terano, "Capsule endoscopy: past, present, and future," *J. Gastroenterol*, vol. 43, pp. 93–99, 2008.

[8] G. Ciuti, A. Menciassi, and P. Dario, "Capsule endoscopy: from current achievements to open challenges," *IEEE Reviews in Biomedical Engineering*, vol. 4, pp. 59–72, 2011.

[9] P. Glass, E. Cheung, and M. Sitti, "A legged anchoring mechanism for capsule endoscopes using micropatterned adhesives," *IEEE Trans. Biomedical Engineering*, vol. 5, pp. 2759–5767, 2008.

[10] M. Quirini, A. Menciassi, S. Scapellato, C. Stefanini, and P. Dario, "Design and fabrication of a motor legged capsule for the active exploration of the gastrointestinal tract," *J. Gastroenterol*, vol. 13, pp. 169–179, 2008.

[11] Y. Liu, M. Wiercigroch, E. E. Pavlovskaia, and H. Yu, "Modelling of a vibro-impact capsule system," *Internat. J. of Mech. Sci.*, vol. 66, pp. 2–11, 2013.

[12] E. E. Pavlovskaia, M. Wiercigroch, and C. Grebogi, "Modeling of an impact system with a drift," *Physical Review E*, vol. 64, no. 5, 2001.

[13] G. Luo, X. Lv, and L. Ma, "Periodic-impact motions and bifurcations in dynamics of a plastic impact oscillator with a frictional slider," *Eur. J. Mech., A, Solids*, vol. 27, no. 6, pp. 1088–1107, 2008.

[14] J.-H. Ho, V.-D. Nguyen, and K.-C. Woo, "Nonlinear dynamics of a new electro-vibro-impact system," *Nonlinear Dynamics*, vol. 63, pp. 35–49, 2011.

[15] A. Depouhon, V. Denoël, and E. Detournay, "A drifting impact oscillator with periodic impulsive loading: Application to percussive drilling," *Physica D*, 2013. Article in press.

[16] M. di Bernardo, C. J. Budd, A. R. Champneys, and P. Kowalczyk, *Piecewise-smooth dynamical systems. Theory and Applications*, vol. 163 of *Applied Mathematical Sciences*. New York: Springer-Verlag, 2004.

[17] P. T. Piiroinen and Y. A. Kuznetsov, "An event-driven method to simulate Filippov systems with accurate computing of sliding motions," *ACM Trans. Math. Software*, vol. 34, no. 3, p. 24, 2008.

[18] B. Krauskopf, H. Osinga, and J. Galán-Vioque, eds., *Numerical Continuation Methods for Dynamical Systems*. Understanding Complex Systems, Netherlands: Springer-Verlag, 2007.

[19] F. Dercole and Y. A. Kuznetsov, "SlideCont: An Auto97 Driver for Bifurcation Analysis of Filippov Systems," *ACM Trans. Math. Software*, vol. 31, no. 1, pp. 95–119, 2005.

[20] H. Dankowicz and F. Schilder, *Recipes for continuation*. Computational Science and Engineering, Philadelphia: SIAM, 2013.

[21] P. Thota and H. Dankowicz, "TC-HAT: A Novel Toolbox for the Continuation of Periodic Trajectories in Hybrid Dynamical Systems," *SIAM J. Appl. Dyn. Sys.*, vol. 7, no. 4, pp. 1283–1322, 2008.

[22] E. J. Doedel, A. R. Champneys, T. F. Fairgrieve, Y. A. Kuznetsov, B. Sandstede, and X.-J. Wang, *Auto97: Continuation and bifurcation software for ordinary differential equations (with HomCont)*. Computer Science, Concordia University, Montreal, Canada, 1997. Available at `http://cmvl.cs.concordia.ca`.

[23] J. Páez Chávez and M. Wiercigroch, "Bifurcation Analysis of Periodic Orbits of a Non-Smooth Jeffcott Rotor Model," *Commun. Nonlinear Sci. Numer. Simul.*, vol. 18, no. 9, pp. 2571–2580, 2013.

[24] J. Páez Chávez, E. E. Pavlovskaia, and M. Wiercigroch, "Bifurcation analysis of a piecewise-linear impact oscillator with drift," *Nonlinear Dynamics*, vol. 77, no. 1-2, pp. 213–227, 2014.

[25] M. Liao, J. Ing, J. Páez Chávez, and M. Wiercigroch, "Bifurcation Techniques for Stiffness Identification of an Impact Oscillator," *Commun. Nonlinear Sci. Numer. Simul.*, vol. 0, no. 0, pp. 0–0, 2015.

[26] E. E. Pavlovskaia and M. Wiercigroch, "Analytical drift reconstruction for visco-elastic impact oscillators operating in periodic and chaotic regimes," *Chaos, Solitons and Fractals*, vol. 19, no. 1, pp. 151–161, 2004.

[27] M. di Bernardo, C. J. Budd, A. R. Champneys, P. Kowalczyk, A. Nordmark, G. Tost, and P. T. Piiroinen, "Bifurcations in nonsmooth dynamical systems," *SIAM Review*, vol. 50, no. 4, pp. 629–701, 2008.